23rd ABCM International Congress of Mechanical Engineering
December 6-11, 2015, Rio de Janeiro, RJ, Brazil

ANALYSIS OF THE BENEFITS OF AN OPTIMIZED VARIALE TRAILING EDGE ON UAV LOITER PERFORMANCE

Vinicius Ayello Deo
Instituto de Aeronáutica e Espaço IAE/CTA
ayellodeo@hotmail.com

Abstract. *A careful analysis of an UAV flight shows a constant limitation on the economic flight regime especially at the loiter phase on intelligence, surveillance, target acquisition and reconnaissance (ISTAR) missions. The maximum endurance flight is limited by the aircraft minimum safety speed, therefore the performance at long typical ISTAR missions, up to 30 hours of flight is compromised. The variable camber wing shows a viable solution to enhance the aircraft's maximum lift coefficient reducing the minimum flight speed limit without major penalty on the drag increase. Through a combined empirical and theoretical analysis, an optimized flap device was designed to enhance the UAV performance at maximum endurance flight by augmenting the wing's maximum lift coefficient with the lowest drag increase possible. An increase of up to 7% on the total flight endurance was estimated at all flight conditions, confirming the benefit of this technology on an UAV design.*

Keywords: *Aircraft performance, Unnamed Air Vehicles, Aircraft Design, Variable Trailing Edge.*

1. INTRODUCTION

The development and research on UAV technology is under constant growth especially on these last decades due to the increase of its usage at the military scenario.

Much has been researched on UAV navigation and control systems, sensors and communication technology but, in contrast with the traditional aeronautics, the platform aerodynamics and performance have not attained sufficient attention from the research community mainly due to the complexity of UAV systems mentioned above and the old idea that the UAV platform is only an useful tool to carry complex and highly technological sensors.

A very interesting characteristic of traditional UAV platforms are the low wing loading along with high aspect ratio wings, mainly due to low speed flight regime and the necessity for high glide ratios. Beyond these two characteristics, the low Reynolds number flight and the sensors generally installed at the platform fuselage contributes for the high parasite drag of the UAV platforms.

These special features of an UAV design are responsible for the optimum flight profile being almost always limited by the platform´s stall speed, therefore the maximum range and maximum endurance flight regimes are not attainable, being constantly limited by the aircraft minimum safety speed.

The variable camber wing is responsible to improve the maximum endurance flight of UAV by increasing the aircraft´s maximum lift coefficient without a major increase on the platform´s drag improving the flight efficiency and increasing the total loiter time.

2. THE UAV PLATFORM

The UAV platform used in this research is the result of a conceptual design for a medium range and long endurance platform for intelligence, surveillance, target acquisition and reconnaissance (ISTAR) missions based on the IAI Heron and Elbit Hermes 900.

Figure 1 – UAV platforms: Hermes 900 and IAI Heron

It is equipped with a 142 hp piston engine and a two blade propeller with 1.91 m of diameter. The piston engine and propeller are typical solutions for this special kind of UAV platform and mission due to the low Mach number cruise and the long endurance flight phase.

Table 1 - Engine Parameters

ENGINE		
POWER	142.76	[hp]
$D_{propeller}$	1.91	[m]
# Blades	2.00	

The design weights are similar to the two UAV platforms in Figure 1 and are characterized by the maximum fuel weight (MUFW) of 317 kgf and capable of carrying a total payload of 280 kgf.

Table 2 – Design Weights

WEIGHT $_{[kgf]}$	
MTOW	1195.16
BOW	597.24
FUEL	317.67
PAYLOAD	280.00

The aspect ratio wing of 20 is essential for the high glide ratio requirements for these UAVs based on the engine failure safety flight. This high aspect ratio contributes to the low total drag of the platform in spite of the high parasite drag estimated as $CD_0 = 0.0367$ as a consequence of the low Reynolds flight ($Re \approx 1.5 \times 10^6$) and the 10% increase in total drag due to excrescence.

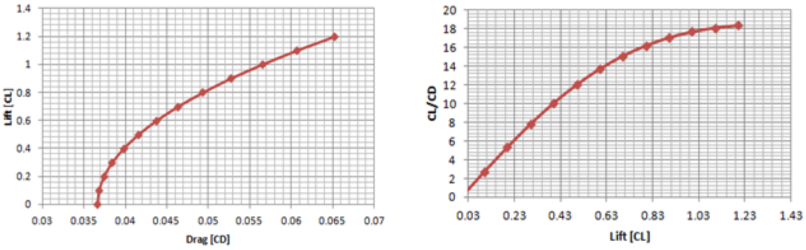

Figure 2 – Estimated new platform aerodynamics

The resulting wing has the characteristically high span and small wing chords typical from high aspect ratios platforms.

Table 3 – Wing Geometry

WING	
$S_{w\,[m2]}$	9.56
$b_{w\,[m]}$	13.83
$Cr_{w\,[m]}$	0.95
$Ct_{w\,[m]}$	0.43
$CMA_{w\,[m]}$	0.72
$Y_{CMA\,[m]}$	3.02

3. THE MAXIMUM ENDURANCE FLIGHT

The typical mission of an ISTAR UAV is the long loiters up to 30 hours at fixed altitude. The best flight regime for this operation is the maximum endurance speed which results in the minimum fuel flow (*FF*) and consequent minimum fuel used at each mission. Considering a cruise flight, the maximum endurance speed (V_{MES}) minimizes the product between the engine's specific fuel consumption (*sfc*), modeled according to (Howe, 2005), and the aircraft total drag.

$$V_{MES} = arg[min(FF)] \therefore FF = sfc \cdot D = sfc \cdot \frac{1}{2}\rho S V^2 CD(CL) \quad (1)$$

The maximum endurance speed determination is a constrained minimization problem since the aircraft speed must lie between the minimum flight speed (V_{min}) and the maximum flight speed (V_{max}) which is limited by engine performance or maximum operational speed (V_{MO}).

$$V_{min} \leq V_{MES} \leq V_{max} \therefore V_{min} = K_{vs} V_{stall} = K_{vs}\sqrt{\frac{2W}{\rho S CL_{max}}} \quad (2)$$

This present work assumes a minimum speed 10% greater than the aircraft stall speed, $K_{vs} = 1.1$ and a maximum lift coefficient for the clean wing of $CL_{max} = 1.2$. This constant factor for the aircraft minimum speed is consistent with the definition of minimum speed presented at STANAG 4671.

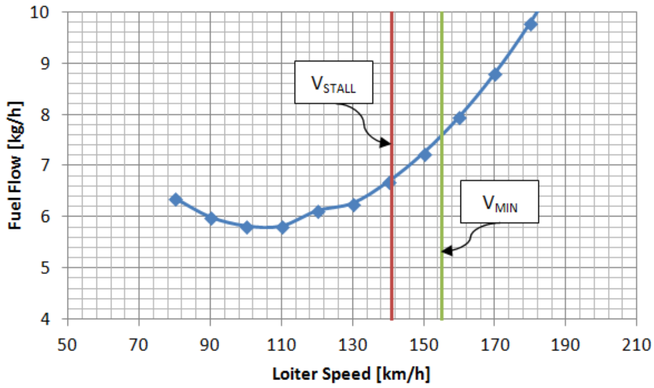

Figure 3 – Fuel Flow at W = 1000 kg, FL050 and ISA+10

At Figure 3 it becomes clear that the maximum endurance performance is usually limited by the aircraft minimum safety speed, therefore the aircraft performance can be improved if these limits become lower by the use of variable camber devices.

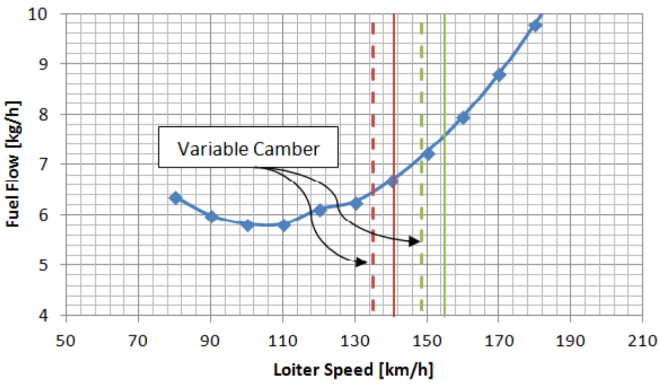

Figure 4 – The effect of variable camber on maximum endurance speed limit

4. MODELLING METHODOLOGY

In order to correctly analyze the effect of variable camber on the maximum endurance performance, the total increase on the wing´s maximum lift coefficient and on total drag must be estimated along with the estimated weight penalty due to the flap system installation.

The variable camber consists of three plain flap panels along the wing´s trailing edge with variable chord, span and flap deflection angle.

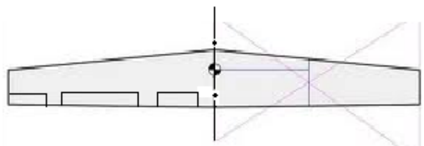

Figure 5 – Trailing edge plain flaps for variable camber

4.1 Maximum Lift Improvement

The maximum lift improvement is modeled according to the ESDU series based on experimental and theoretical data and is dependent on airfoil and wing parameters.

$$\Delta CL_{max} = F_R \left(\frac{\Delta CL_{mt}}{\mu}\right)(\phi_o - \phi_i) \quad (3)$$

The parameters ϕ_0 and ϕ_t account for part span flap panel and are tabulated according to the position of the inboard and outboard flap. The coefficient μ is the ratio of the wing local section peak lift coefficient to the total wing coefficient and is dependent on wing geometry. A correction is made based on the aircraft Reynolds number.

$$F_R = 0.153 \times log(Re) \quad (4)$$

The section maximum lift increment ΔCL_{mt} is derived by theoretical analysis based on thin airfoil theory corrected with experimental data.

$$\Delta CL_{mt} = K_G K_t T \Delta CL_0 \quad (5)$$

The variable ΔCL_0 is the section maximum lift increment at zero angle of attack and is modeled based on flap geometry and deflection angle.

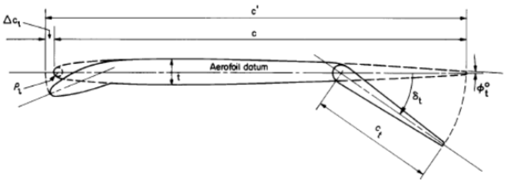

Figure 6 – Airfoil geometry parameters

$$\Delta CL_0 = 2J_p\delta_t \left\{\pi - acos\left(2\frac{c_t}{c} - 1\right) + \sqrt{\left[1 - \left(2\frac{c_t}{c} - 1\right)^2\right]}\right\} \quad (6)$$

The parameters K_G, K_t, T and J_p are correction factors experimentally tabulated as functions of flap and airfoil geometry.

4.2 Parasite Drag Increment

The parasite drag increment due to the deployment of the trailing edge flaps were calculated based on experimental data as a function of flap chord and area ratio and deflection.

$$\Delta CD_{0,w} = \frac{Sf}{S}\Delta CD_0 \quad (7)$$

The value of ΔCD_0 is experimentally derived and can be found graphically according to **Figure 7**. If the flap deflection angle is smaller than 8^o an empirical correlation is used, according to Eq. 8.

$$if\ \delta_f \leq 8^o,\ \Delta CD_0 = 1.29\left(\frac{c_f}{c}\right)^{1.25} sin^2(\delta_f) \quad (8)$$

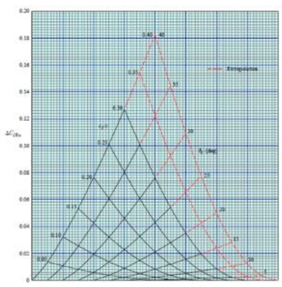

Figure 7 – Profile drag increment

4.3 Induced Drag

The induced drag penalty is calculated based on theoretical modeling using Prandt Lifting Line solution. Considering a straight tapered wing, the total induced drag is estimated as a function of the aspect ratio and the Fourier coefficients A_n.

$$CD_i = \pi A \sum_{n=1}^{N} n A_n^2 \tag{9}$$

For a wing with trailing edge flaps deployed, the coefficient A_n can be expressed as dependent on the angle of attack and flap deflection.

$$A_n = a_n(\alpha - \alpha_0) + c_n \delta_f \tag{10}$$

The parameters a_n and c_n are the solutions of the matrix equations below.

$$\sum_{n=1}^{N} a_n \left[\frac{4b}{CL_\alpha c(\theta)} + \frac{n}{\sin(\theta)}\right] \sin(n\theta) = 1;\ \sum_{n=1}^{N} c_n \left[\frac{4b}{CL_\alpha c(\theta)} + \frac{n}{\sin(\theta)}\right] \sin(n\theta) = \chi(\theta) \tag{11}$$

On a straight tapered wing, the chord distribution along the span is calculated as a function of the parameter θ, the wing aspect ratio (A) and taper (λ).

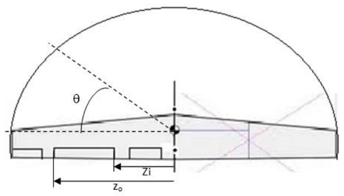

Figure 8 – Chord Location Parameter

$$c(\theta) = \frac{2b}{A(1+\lambda)}[1 - (1-\lambda)|\cos(\theta)|] \tag{12}$$

The variable $\chi(\theta)$ is the distribution along the wing span of flap effectiveness. The flap effectiveness is calculated theoretically by the thin airfoil theory and corrected by empirical derived factors.

$$\chi(\theta) = \begin{cases} 0 & z < z_i \\ \varepsilon_f = \eta_h \eta_d \left\{1 - \frac{acos\left(2\frac{c_f}{c}-1\right) - sin\left[acos\left(2\frac{c_f}{c}-1\right)\right]}{\pi}\right\} & z_i < z < z_o \\ 0 & z > z_o \end{cases} \tag{13}$$

The values of the empirical variables η_h, hinge efficiency, and η_d, deflection efficiency, are dependent on flap chord ratio (c_f/c) and deflection (δ_f) according to (Phillips, 2010).

Since the interest is on the drag increment caused by the flaps deflection, assuming as a premise an elliptical wing loading, the following approximation can be made.

$$\Delta CD_i = \pi A \left\{\sum_{n=1}^{N} n\left[a_n(\alpha-\alpha_0) + c_n\delta_f\right]^2 - \sum_{n=1}^{N} n[a_n(\alpha-\alpha_0)]^2\right\} \cong \pi A \sum_{n=1}^{N} n\left(c_n\delta_f\right)^2 \tag{14}$$

4.4 Weight Increment

The increase of the aircraft weight due to flap system installation is difficult to correctly predict at the conceptual design phase. It is usual to estimate the weight penalty using empirically derived relations. According to (Torenbeek, 1976) the weight increment is calculated as function of flap geometry, deflection and its design speed, here assumed as $1.8V_{stall}$.

$$\Delta W = \left\{2.706\left(S_f b_f\right)^{3/16}\left[\left(\frac{1.8V_{stall}}{100}\right)^2 \frac{sin(\delta_{f,max})}{(\frac{t}{c})_f}\right]^{3/4}\right\} S_f \tag{15}$$

The above correlation has the assumption of a wing without sweep angle and the values of $(t/c)_f$ of 0.1 and $\delta_{f,max}$ of 20º were used during the calculation process, with S_f and b_f being the flap area and span respectively.

4.5 Calculation Procedure

The total drag, maximum lift and weight increment are used in the performance calculation module to modify the stall speed limit and the aircraft fuel flow which will result on different values of the aircraft total loiter time, therefore being able to be optimized to find the best flap geometry that maximizes the aircraft flight time.

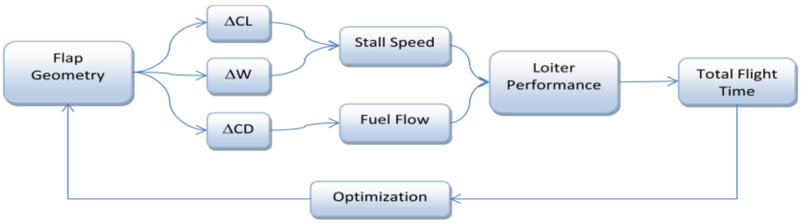

Figure 9 – Calculation and optimization Procedure

5. OPTIMIZATION

The optimization objective is the total flight time augmentation by the deployment of trailing edge flaps and modifying its geometry at each integration time step. The main expected results are the design of a variable camber flap that maximizes the UAV loiter in order to enhance its performance on intelligence, surveillance, target acquisition and reconnaissance (ISTAR) missions.

5.1 Variables

A total of 12 variables regarding the flap geometry were considered on the optimization process. The three flap panels span, chord and deflections.

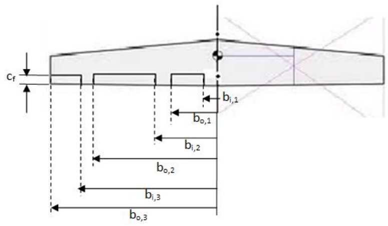

Figure 10 – Optimization Variables

The complete set of optimization variables are summarized on the vector below.

$$\boldsymbol{X} = [b_{i,1;}\ b_{o,1;}\ b_{i,2;}\ b_{o,2;}\ b_{i,3;}\ b_{o,3;}\ c_{f,1;}\ c_{f,2;}\ c_{f,3;}\ \delta_{1;}\ \delta_{2;}\ \delta_3] \quad (16)$$

5.2 Constraints

The optimization variables have geometrical constraints that must be satisfied during the optimization process. These constraints are responsible to control the optimization algorithms so it does not violate geometry restrictions such as flaps overlapping and the variable bounds.

The lower bound constraint for the three flap spans are 0 m, corresponding to a wing without flap panels, the minimum value for the flap chord ratio is 5% of the wing´s chord and a minimum deflection of 0º for all three panels.

$$\boldsymbol{LB} = [0; 0; 0; 0.05; 0.05; 0.05; 0; 0; 0] \quad (17)$$

The upper bound constraints for these variables are the wing span for the flap panels, 50% of the wing chord and a maximum flap deflection of 20º.

$$\boldsymbol{UB} = [b; b; b; 0.5; 0.5; 0.5; 20; 20; 20] \quad (18)$$

The last sets of constraints are geometrical limitations of the three flap panels to prevent flap overlapping.

$$\begin{bmatrix} 1 & -1 & 0 & 0 & 0 & 0 \\ 0 & 1 & -1 & 0 & 0 & 0 \\ 0 & 0 & 1 & -1 & 0 & 0 \\ 0 & 0 & 0 & 1 & -1 & 0 \\ 0 & 0 & 0 & 0 & 1 & -1 \end{bmatrix} \begin{bmatrix} b_{i,1} \\ b_{o,1} \\ b_{i,2} \\ b_{o,2} \\ b_{i,3} \\ b_{o,3} \end{bmatrix} \leq \begin{bmatrix} 0 \\ 0 \\ 0 \\ 0 \\ 0 \end{bmatrix} \tag{19}$$

5.3 Algorithm

A hybrid optimization algorithm was used in series, first a genetic algorithm explores the complete solution space to find the region of the most probable solution to the optimization problem, and then a hessian based algorithm tries to optimize the objective function starting around that most feasible point using the thrust region concept.

The genetic algorithm evaluates a population of 120 individuals corresponding to 10 times the number or variables over 500 generations. The stopping criteria used was a function tolerance of 10^{-4}.

The subsequent optimization algorithm used central finite difference to evaluate the derivatives and a maximum of 3000 function evaluation and tolerance of 10^{-8} as stopping criteria.

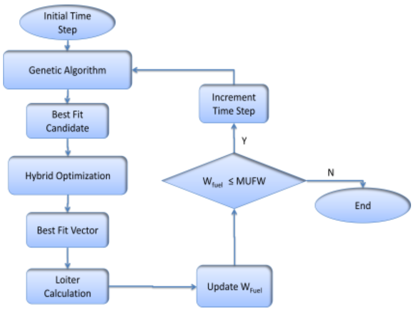

Figure 11 – Optimization Flowchart

The optimization process occurs at every integration time step until the total fuel burned W_{Fuel} is equal to the maximum usable fuel weight MUFW.

6. RESULTS

A total of three conditions of loiter performance were analyzed during the optimization process.

Table 4 – Loiter Conditions

Loiter Conditions	
W [kg]	1000
ΔISA [°C]	10
Hp [ft]	5.000
	10.000
	15.000

For every condition, the performance benefit of the variable camber at the loiter phase, expressed by the increase on total flight time, was analyzed, besides the aerodynamic improvement (ΔCL/ΔCD) and the breakdown of total drag increase in terms of induced and parasite drag.

The optimization process resulted on full span flap deflections close to 10.5° and a flap chord ratio around 7.5%.

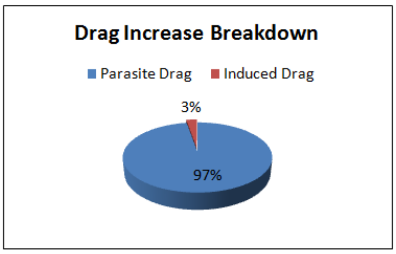

Figure 12 – Drag increase breakdown

These conditions correspond to a total lift augmentation of 0.18, 15% of the clean wing maximum lift coefficient and a total drag increase of approximately 0.0014 (14 drag counts) which is roughly 4% of the aircraft´s parasite drag.

The performance benefits of the variable camber showed an increase on total flight time at maximum endurance speed of 6-7%, improving the UAV mission capability reaching an optimized flight regime.

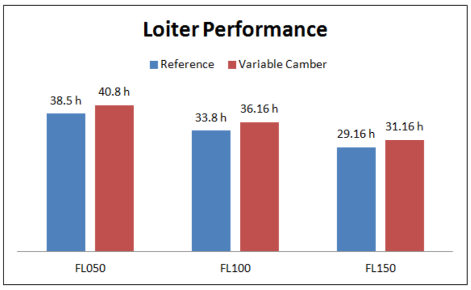

Figure 13 – Variable Camber Benefits on Loiter Performance

7. CONCLUSION

The benefits of the variable camber device on the loiter performance may be as high as a 7% increase on total flight time. Besides the improvement on holding performance, which is essential on ISTAR missions, the same process and technology may be used to optimize other flight regimes such as climb and cruise phases where the maximum range flight speed is not attained on the majority of UAV cruise conditions. It is a fairly simple and reliable technology where great benefits may be attained on UAV flights due to its special operation characteristics which make it distinct from conventional aircraft operations.

8. REFERENCES

Garner et al. ESDU 91014: Maximum Lift of Wings with Trailing-Edge Flaps at Low Speeds. London: The Royal Aeronautical Society, 1991

Garner et al. ESDU 94028: Increments in Aerofoil Lift Coefficient at Zero Angle of Attack and in Maximum Lift Coefficient due to Deployment of a Plain Trailing-Edge Flap, with or without a Leading-Edge High-Lift Device, at Low Speeds. London: The Royal Aeronautical Society, 2004

Howe, Denis. Aircraft Conceptual Design and Synthesis. Delhi: Wiley, 2000.

Phillips, Warren. Mechanics of Flight. 2. ed. Delhi: Wiley India, 2010.

Torenbeek, Egbert. Synthesis of Subsonic Airplane Design. Delft: Delft University Press, 1976.

Wells et al. ESDU 06014: Zero-Lift Drag Coefficient Increment Due To Full-Span Plain Flaps. London: The Royal Aeronautical Society, 2006.

Young et al. ESDU Flaps 02.01.08: Vortex Drag Coefficient Of Wing With Part-Span Flap And Central Cut-Out. London: The Royal Aeronautical Society, 2013.

9. RESPONSIBILITY NOTICE

The author is the only responsible for the printed material included in this paper.